Sealing Performance of a Turbine Rim Chute Seal Under Rotationally-Induced Ingestion

Sealing Performance of a Turbine Rim Chute Seal Under Rotationally-Induced Ingestion

Anna Bru Revert[1], Paul F. Beard[1], John W. Chew[2], Sebastiaan Bottenheim[3]

[1] Oxford Thermofluids Institute, Dept.Engineering Science, University of Oxford, Oxford, OX2 0ES, UK
[2] Thermo-Fluid Systems UTC, Dept.Engineering and Physical Sciences, University of Surrey, Guildford GU2 7XH, UK
[3] Rolls-Royce plc, PO Box 3, Bristol, BS34 7QE, UK

Corresponding author: anna.brurevert@eng.ox.ac.uk

Abstract. *This study focuses on the sealing capability of a turbine rim seal subject to hot gas ingestion driven purely by the rotor disc pumping effect rather than that induced by mainstream features such as vane and rotor blade passing. The aim is to provide useful data for conditions in which rotation dominates, and to clarify the flow physics involved in rim sealing. Experimental measurements of sealing effectiveness for a chute seal are presented for the first time without and with an axial, axisymmetric mainstream flow external to the seal. The test matrix covers a range of rotational Reynolds number,* Re_ϕ*, from* $1.5x10^6$ *to* $3x10^6$*, and non-dimensional flow rate,* C_w*, from 0 to* $4x10^4$ *with the mainstream flow (when present) scaled to match engine representative conditions of axial Reynolds number,* Re_{ax}*. Results from steady pressure and gas concentration measurements within the rotor-stator disc cavity and the rim seal gap are presented and compared to published data for other seal designs. Sealing performance of the chute seal is somewhat similar to that of axial clearance seals with the same minimum clearance.*

1. Introduction

Up to 25% of the intake mass flow in gas turbine engines is channeled from the compressor through a secondary air system, bypassing the combustion chamber and re-entering the main gas path at various points in the turbine. The coolant air is of paramount importance to the integrity and reliability of the hot section components throughout their operating life, but the amount of air bled from the compressor must be optimised to limit the thermodynamic efficiency penalty.

A small gap in the turbine annulus hub line is required to allow for the relative radial and axial movement of the rotor blades and the nozzle guide vanes (NGVs). However, this necessary clearance must be sealed with a portion of the secondary air to prevent hot gas exiting the combustor from entering the stator-rotor disc volume. To assist the sealing process, engine designers often include a lip at the periphery of the stator disc that protrudes into the gap, known as rim seal, providing blockage to entrainment of external flow into the cavity. In recent years, gas turbine designers have gained awareness of the complexity of the interaction between the sealing air flow and the main gas path air, both at the rim seal and in the cavity below. Hence, interest in improving the understanding of the physics of sealing flows has significantly increased with the aim of developing more robust and accurate design models.

2. Literature review

Early studies in rim sealing flows aimed to quantify the minimum flow rate necessary to completely isolate simple cavity geometries from a quiescent external environment, Bayley and Owen [1]. This led to empirical correlations of the minimum non-dimensional flow rate required to fully seal the cavity, $C_{w,min}$, from what is now known as rotationally-induced ingestion. Further experimental studies on rotationally-induced ingestion provided data for a number of seal types, and use of gas concentration measurements allowed sealing effectiveness for flow rates $C_w < C_{w,min}$ to be quantified. A rotating disc immersed in a fluid imposes its rotation to the surrounding fluid. Consequently, the flow in the boundary layer on the rotating disc will be ejected radially outwards owing to the centrifugal force. This phenomenon is referred to as the disc pumping effect. Considering the flow in the turbine disc cavity to be largely controlled by disc pumping, Chew [2] developed an orifice model to correlate research data and estimate sealing effectiveness for different seal designs in the absence of external annulus flow. For small seal clearances, as considered in the present study, results from this model are approximated by Eq. 1 in which the value of the empirical constant k depends on the geometry of the rim seal, providing a measure of the seal's ability to inhibit ingestion into the cavity.

$$\frac{U_{m,min}}{\Omega b} = 0.1214\,k; \qquad \varepsilon = \frac{1}{0.8 + 0.02428\,k\,\left(\Omega b/U_m\right)} \quad for\ 0 < U_m < U_{m,min} \qquad \text{Eq. 1}$$

Here U_m, Ω and b denote the mean velocity through the seal, rotor angular speed, and radial location of the seal. The sealing effectiveness ε is based on concentration of a tracer gas in the cavity.

Chew *et al.* [3] estimated the value of k for axial and radial seals and fitted the model to their own experimental data finding good agreement also with results from other research groups in absence of mainstream flow. For $k = 0.8$, the model gives $C_{w,min} = 0.61\,s_c \mathrm{Re}_{\emptyset}$, where s_c is the non-dimensional seal clearance, resulting in Bayley and Owen's correlation for a simple axial clearance seal.

Abe *et al.* [4] showed that the turbine main annulus flow, specifically the pressure and velocity potential field asymmetries introduced by the stator vanes, play a key role in ingestion of mainstream flow. Phadke and Owen [5] then investigated the effect of external flow (in quasi-axisymmetric and non-axisymmetric conditions) concluding that the ingestion of hot mainstream gas into the stator-rotor cavity can be rotationally-induced, or externally-induced (when driven by the pressure asymmetries in the main gas path).

Green and Turner [6] investigated the influence of NGVs and rotor blades and they found that the introduction of the rotor blades aided the sealing of the cavity by smoothing out the potential field of the NGVs. Further studies emphasised the role of the NGVs and the rotating blades. In their review paper, Johnson *et al.* [7] listed rotor disc pumping, periodic pressure field in the annulus, geometrical 3D features within the rim seal region, asymmetries in the rim seal geometry, turbulent transport and flow entrainment as the main mechanisms that influence rim seal ingestion. Some years after Johnson *et al.*'s review, Cao et *al.* [8] presented a combined CFD and experimental study identifying large-scale unsteady flow features (unrelated to blade passing frequencies) as a key mechanism for gas ingestion into the axial gap between the rotor and stator discs. CFD solutions indicated that these flow structures and the ingestion were rotationally-driven. The rotating flow modes are interpreted as inertial waves and may originate within the seal. Extensive reviews of turbine rim sealing have more recently been given by Scobie *et al.* [9] and Chew *et al.* [10].

The current investigation focuses on understanding the flow physics of rim sealing exclusively under rotationally-induced ingestion with a bladeless gas path. The conditions considered do not reproduce the more hostile environment found in a gas turbine engine but are chosen to allow a more fundamental study of the physical principles that drive the flow behavior. To the authors' knowledge, this is the first time that rotationally-induced ingestion is reported for a chute seal geometry.

A brief description of the experimental set up, instrumentation and test matrix is included. Next, the mean cavity flow behavior is described followed by a comparison of the data obtained during this investigation against other published experimental data and analytical correlations. An analysis of the cavity flow behavior based on pressure measurements is conducted. Finally, the sealing performance of the chute seal is assessed under different test conditions based on sealing effectiveness data.

3. Oxford Rotor Facility – Experimental Set up

The experimental data reported in this study was acquired in the Oxford Rotor Facility (ORF), recently modified to focus on turbine secondary air systems research. An extended run time of duration of minutes was achieved through an annulus line of reduced radial span to minimise the required mainstream mass flow rate in combination with a new air supply system.

3.1. Mainstream reduced annulus and air supply systems

The casing annulus line radius was decreased to 20% of its original radial span to increase the test time of the facility – see Figure 2(a). The axial Mach number above the rim seal at the exit of the NGVs was matched to the previous engine-representative operating conditions of the ORF ($M = 0.34$). A casing was designed to minimise pressure loss, with sufficient annulus height to allow representative interaction between mainstream and cavity purge flows. Ambient air at 27.6 bar was supplied to the test section through the parallel connection of a flow limiter and a pressure reducing valve, Figure 1(a). This configuration provided constant pressure upstream of separate ISO9300:2015 compliant choked nozzles (uncertainty in C_d = ±0.5%) supplying constant mass flux conditions to the mainstream and purge streams. The annulus flow was initiated by an actuated ball valve upstream of parallel metering nozzles that controlled the flow of mainstream air before it entered an inlet flow distributor and the turbine test section.

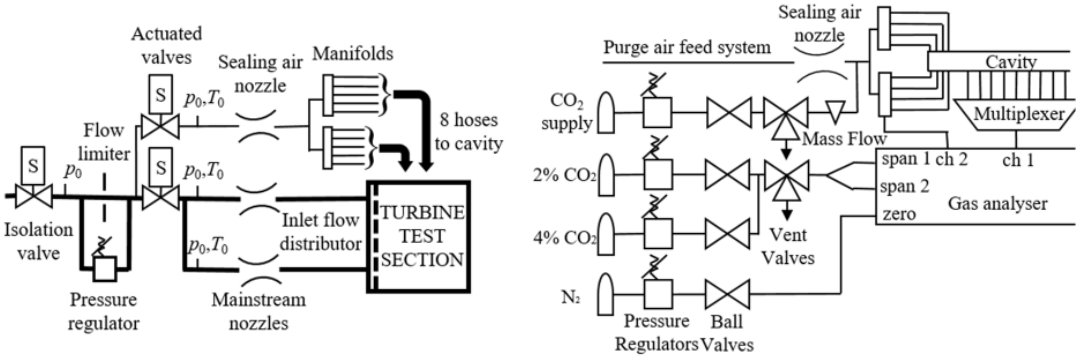

(a) (b)

Figure 1: (a) Mainstream and purge air feed supply, (b) Sealing effectiveness measurement system.

The purge flow passes through a single metering nozzle and then into a manifold that distributes the flow through 8 flexible hoses, which are connected evenly around the circumference of the facility, to an annular settling volume in the working section. In the absence of annulus flow and for low sealing flow rates ($\dot{m}_{purge} <$ 0.035 kg s^{-1}), the purge flow was instead metered by an Alicat MC Series 2000 mass flow controller, with a traceable uncertainty of ±0.8% of reading plus ±0.2% of full scale. Together with the previously described reduced annulus area, a steady test time of up to 20 minutes was possible.

3.2. Rim seal geometry

Details of the working section geometry adopted for this study are presented in Figure 2(a). Without blading, the rotor hub platform (1) and the hub vane ring (2) were solid, axisymmetric rings that defined the rim seal design. The ORF includes a split disc (3) allowing modification to the rotor seal geometry by simply replacing the rotor hub platform component. The potential leak path between the rotor disc and rotor hub platform is sealed using flexible silicone.

The chute seal design used in this study is identical to that used by Beard *et al.* [11]. The nominal seal clearance was designed to be 1 mm at the maximum rotor disc speed of 9000 rpm. The radial growth of the rotor disc was previously evaluated by Beard *et al*. and accounted for in this study. Introducing a spacer ring between the disc and the shaft increased the distance between the stator and rotor ring, leading to a seal gap of 1.85 mm. The larger seal gap simulates a potential engine off-design condition, where the relative axial displacement between static and rotating components may vary. It is

worth highlighting that from a 2 mm axial overlap, opening the seal clearance led to a 0.5 mm axial seal gap instead.

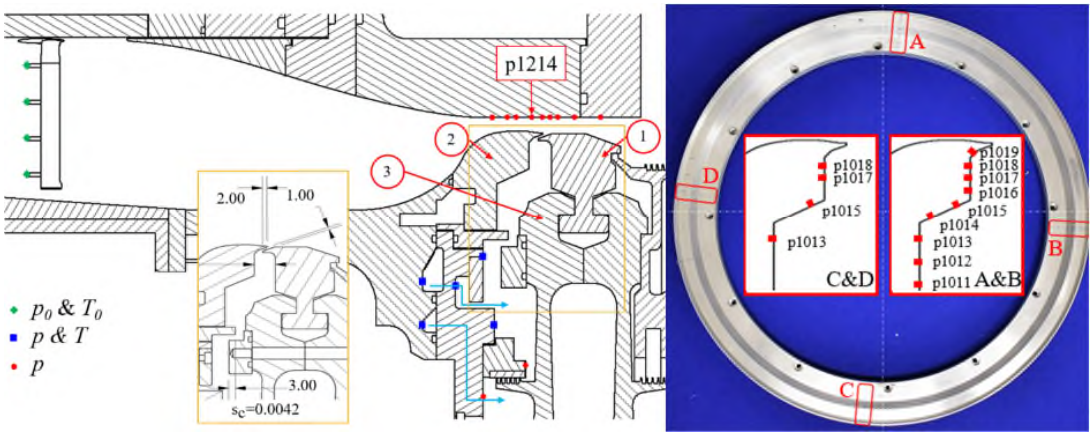

(a) (b)

Figure 2: (a) Sectional view of ORF working section with measurement locations and chute seal geometry details, (b) Rim seal cavity measurement positions.

3.3. Instrumentation

Static pressure and gas temperature measurements were acquired extensively through the working section, including: the mainstream annulus, purge flow feed system and the rotor disc and rim seal cavities. All data was sampled at 200 Hz by a National Instruments PXI/SCXI data acquisition system.

3.3.1. Steady pressure and temperature

All steady pressure measurements were obtained by pneumatic pressure transducers connected to 1.6 mm diameter tappings with flexible vinyl tubing. Absolute measurements were acquired using First Sensor CTE8000 transducers with a nominal uncertainty of ±0.1% of the full-scale output. All gas temperature measurements were obtained using k-type bare bead (d = 76.2 µm) thermocouples (±0.45% uncertainty).

The measurement locations in the purge flow feed system, rotor cavity and stator wall are shown in Figure 2(a) and Figure 2(b). Radial distributions of static pressure tappings were installed at four locations, distributed evenly around the cavity. At locations A & B nine points extended across the radial span of the cavity, whereas at locations C & D a lower resolution of four repeat measurements was included. The static pressure data were acquired by First Sensor BTEM5000 0-100 mbar unidirectional differential pressure transducers with a nominal uncertainty of ±0.2% (or ±0.2 mbar) of the full-scale output. Measurements were referenced to the innermost measurement location (p1011).

Upstream mainstream total pressure, p_0, and temperature, T_0, were measured using radial rakes, each including 4 pitot tubes or four k-type bare bead thermocouples (±0.45% uncertainty) at 90º intervals respectively. The annulus static pressure p was sampled at nine axial positions on the reduced annulus casing wall above the seal. The flow velocity in the annulus was calculated from these measurements of p_0, p and T_0.

3.3.2. Sealing effectiveness measurement system

The tracer gas technique consists of seeding the purge flow with a foreign gas, commonly carbon dioxide, whilst the mainstream flow is kept at atmospheric composition. A CO_2 concentration in the purge air of 3% was used in this study. Measurements of tracer gas concentration in the air mixture then indicated ingestion when the concentration fell below that supplied to the cavity, meaning that the extra air from the mainstream diluted the air-CO_2 mixture. The performance of the seal against ingestion can be quantitatively represented by the sealing effectiveness which can take values between 0 (100% ingestion – solely mainstream flow) and 1 (no ingestion – solely purge flow).

$$\varepsilon_c = \frac{c_{stator} - c_{ann}}{c_{purge} - c_{ann}} \quad \text{Eq. 2}$$

CO_2 concentration measurements were acquired using a dual channel Pulsar IV Non-Dispersive Infra-Red multi-gas analyser from Signal Group with linearity and repeatability below ±0.5% and ±0.1% of full scale respectively. A schematic of the sealing effectiveness measurement system is shown in Figure 1(b). A multiplexer allowed sequential sampling of up to 20 measurement points through channel 1, whilst channel 2 continuously monitored the concentration of the purge air at the entry of the rim seal cavity. A constant input of nitrogen purged the measurement sensors expelling the sample gas, as well as defining the zero concentration calibration point. Compressed gas bottles of certified CO_2-air mixtures of 2% and 4% CO_2 concentration (±1% uncertainty in concentration percentage) completed a three-point calibration curve performed daily before the start of testing.

Preliminary tests during commissioning of the new system demonstrated that the air and carbon dioxide in the purge flow were fully blended and the gas mixture entering the cavity through the distribution manifold was homogeneous. The CO_2 mass flux was set by an Alicat MCR mass flow controller and recorded as a 0-5V proportional output signal. The quoted accuracy for the mass flow controller is ±0.8% of reading plus ±0.2% of full scale.

Measurements of CO_2 concentration were taken at nine radial positions along the stator wall of the rim seal cavity (c_{stator}) – using the static pressure tappings at location B in Figure 2(b) – along with the concentration of the mainstream annulus flow (c_{ann}) – static pressure tapping p1214 in Figure 2(a) – and the seeded purge flow (c_{purge}) – monitored for reference at the entry of the test section. The associated absolute uncertainty with the sealing effectiveness measurement was ±0.068 (repeatability error of ±8.4x10^{-3} that provided good ability to measure differences between test cases).

3.3.3. Test matrix

The performance of a turbine rim seal operating under rotationally-induced ingestion may be sensitive to changes in seal geometry, seal clearance, purge flow rate, rotational speed, presence of external (axial) annulus flow, inner cavity geometry, non-uniformities in the annulus, eccentricity and vibrations. The present study focuses on the limiting case of rotationally-driven ingestion for the chute seal. As in many other rim seal studies, eccentricity, vibrations and unintended circumferential asymmetries in the external flow will only arise from practical limits on rig design and manufacture. Although these will be small, the possibility of some influence on the finer detail of the results cannot be ruled out.

The effect of purge mass flow, rotor disc speed, rim seal gap size and annulus mass flow were investigated, analysed and presented in terms of the non-dimensional parameters: non-dimensional (purge) mass flow, C_w; rotational Reynolds number, $\mathrm{Re}_\emptyset$; non-dimensional seal clearance, s_c, and mainstream Reynolds number, Re_{ax}. The test range covered by each of the non-dimensional parameters is summarised in Table 1. The presence of axial mainstream annulus flow is indicated with the axial Reynolds number. Low bandwidth data and gas concentration measurements were acquired at all test conditions. It is worth highlighting that in the $\mathrm{Re}_{ax} = 0$ sealing effectiveness test campaign, the annulus was vented with a weak axial flow to avoid build up of CO_2 above the rim giving false readings.

Table 1: Experimental test matrix

Re_{ax}	C_w	$\mathrm{Re}_\emptyset$	s_c
0	800 to 9000	1.5x10^6 2.1x10^6	4.2x10^{-3}
2.6x10^5	800 to 40000	2.7x10^6 3x10^6	7.8x10^{-3}

4. Mean cavity flow structure

This section provides insight into the flow structure within the rim seal cavity when subjected to purely disc-pumping in the absence of mainstream flow and blading and when axial axisymmetric annulus flow is included.

4.1. Steady cavity flow behaviour

The radial static pressure profile on the stator wall, shown in Figure 3(a), provides a measure of the vortex strength in the rim seal cavity. The pressure coefficient is calculated as the pressure difference to the innermost measurement point available in each test case, non-dimensionalised using the dynamic head at the disc rim speed. In comparison to Beard *et al.* [11], this study was performed with a modified disc clamping arrangement to remove the influence of exposed disc bolts, a reduced casing annulus line and with measurements extended inboard from p1016 to position p1011 in Figure 2(b). Although not showed here, excellent agreement of the cavity pressure measurements between these test campaigns provided evidence that the mean flow aerodynamics beneath the hub remained unaffected by the various changes to the working section.

The extended measurements included in this study ($r/b < 0.94$) reveal a change in slope in the radial distribution of C_p showing two different swirl velocities for the inner and outer parts of the cavity. Lines corresponding to forced vortices at several fractions of disc speed are also shown in Figure 3(a). In a shrouded plane disc rotor-stator system with separate turbulent boundary layers on the rotor and stator, the rotating core between the boundary layers typically rotates at ~ 43% of the rotor disc speed. The results in Figure 3(a) are consistent with this, but show some effects of the non-planar geometry in the stator wall ($0.91 < r/b < 0.94$). A reduction in vortex strength in this region is consistent with an increased surface area (per radial distance) for stator drag.

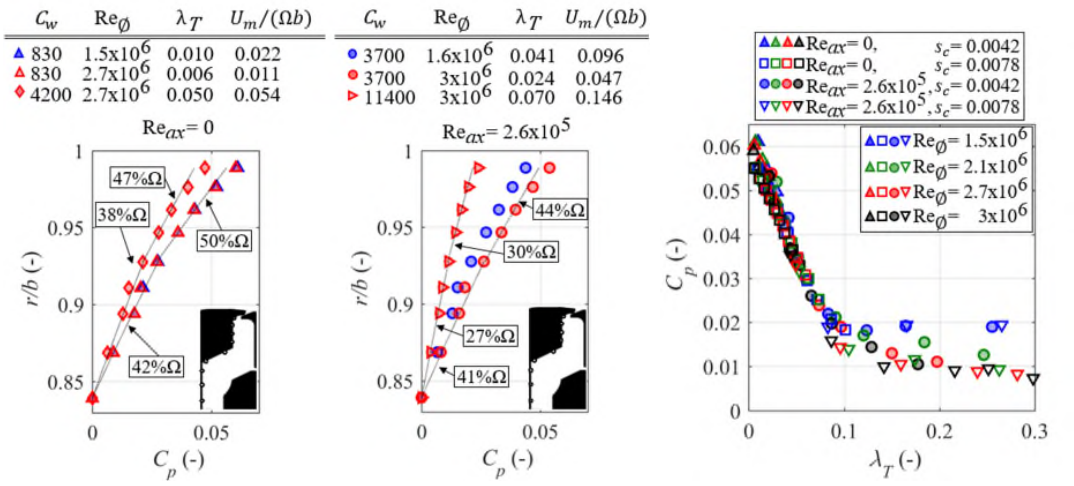

(a) (b)

Figure 3: (a) Effect of C_w, $\mathrm{Re}_\emptyset$ and Re_{ax} in the radial distribution of mean pressure coefficient in rim seal cavity for $s_c = 0.0042$, (b) Effect of the external flow, $\mathrm{Re}_\emptyset$ and s_c in the mean pressure coefficient at the rim, $r/b = 0.99$, correlated against the turbulent flow parameter.

The turbulent flow parameter, $\lambda_T = C_w/\mathrm{Re}_\emptyset^{0.8}$, has previously been shown to characterise the flow in rotor-stator disc cavities. The individual effect of the purge flow rate and rotational Reynolds number in the turbulent flow parameter is analysed in Figure 3(a) for the two annulus flow configurations under consideration. In absence of annulus flow and for a low supply of purge flow, Figure 3(a) left reveals that doubling the rotational Reynolds number appears to have a negligible effect in the radial pressure distribution. For a constant rotor disc speed however, an increase in the purge flow aids the pressurization of the volume, reducing the pressure gradient along the stator wall and providing better sealing. The introduction of mainstream annulus flow, Figure 3(a) right, exacerbates the effects of C_w and $\mathrm{Re}_\emptyset$ in the pressure coefficient. The pressure gradient across the cavity increases with rotational Reynolds number thus increasing the strength of the vortices. Again, a larger supply of purge flow aids the sealing capability of the chute seal and suppresses the rotating core in the cavity.

The mean pressure coefficient, C_p, at the outer measurement location p1019 is plotted in Figure 3(b) against the turbulent flow parameter, λ_T, across the full range of test conditions defined in Table 1.

For values of $\lambda_T < 0.1$, the data collapse to a linear regression regardless of the rotational Reynolds number, seal clearance or the presence of axial flow in the annulus. As the supply of purge flow increases, the swirl velocity in the cavity reduces and a more uniform radial pressure profile is generated on the stator cavity wall – see Figure 3(a). Consequently, the pressure difference across the cavity reduces with increasing turbulent flow parameter.
Interestingly, Figure 3(b) reveals that after the initial linear regression, the pressure coefficient tends to an asymptotic value of $C_p \approx 0.01$ for $\mathrm{Re}_\emptyset > 2\mathrm{x}10^6$. A similar trend is observed for the lowest rotational Reynolds number of $\mathrm{Re}_\emptyset = 1.5\mathrm{x}10^6$, although the pressure coefficient establishes at approximately $C_p \approx 0.02$. For a sufficiently high value of λ_T, the purge flow supplied is enough to overcome the disc pumping, and recirculation of the swirling flow and vortex in the cavity are suppressed. Estimates of free disc pumping with allowance for the effect of a non-zero inner radius of the disc are consistent with a change of flow behavior at $\lambda_T \approx 0.1$. Beyond this value, for $C_p < 0.02$ other effects contribute to the flow structure. Free vortex flow might be expected for $\lambda_T > 0.1$.

5. Sealing performance

This section presents results of sealing effectiveness with and without an axial annulus flow, including comparison to other seal types and the disc pumping model by Chew [2].

5.1. Comparison to previous work

Several geometries under pure disc pumping effect have been explored by other research groups, although purely rotationally-induced ingestion has not previously been reported for a chute seal of the type considered here. Results of sealing effectiveness for the ORF chute seal are plotted in Figure 4(a) (blue circles) as a function of the seal-to-rotor rim velocity ratio, $U_m/(\Omega b)$, also referred as non-dimensional flow ratio.

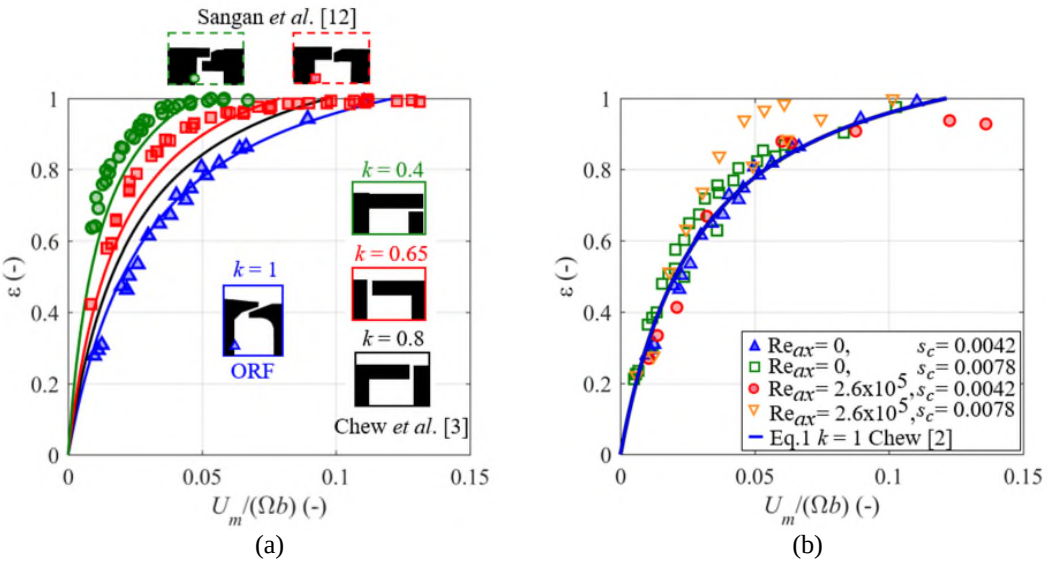

(a) (b)

Figure 4: (a) Comparison of different seal geometries in the distribution of sealing effectiveness against seal to rotor rim velocity ratio, (b) Effect of the annulus flow in the sealing effectiveness as a function of the non-dimensional flow ratio at $r/b = 0.96$ for two different gap sizes.

Figure 4(a) also includes experimental data from Sangan *et al*. [12] for an axial seal (red squares) and radial seal (green triangles). Correlation curves derived by Chew [2] – see Eq. 1 – for rim seal performance exclusively under the disc pumping effect are also plotted for various parameter k values. All experimental results show a similar trend shape for the variation of seal effectiveness to the disc pumping model. For the radial seal tested by Sangan *et al*., the data fall close to the model with $k = 0.4$ as associated with the earlier results used by Chew *et al*. [3] to correlate a simple radial clearance seal. Chew correlated data for two different axial seal geometries (as depicted in Figure 4(a) with solid lines)

with associated k values of 0.65 and 0.8 depending on whether the overhang lip protruded from the stator or rotor wall. For the axial seal tested by Sangan *et al.*, the experimental data shows significantly better sealing performance that the model. This could be due to the difference in seal geometries or possible re-ingestion of purge air from the annulus in these experiments associated with incomplete venting of the annulus space.

As the chute seal includes both radial and axial variation its performance may be expected to lie between that of the axial and radial seals, as demonstrated by Phadke and Owen [5] for their 'mitered' seal. However, results indicate that the chute seal performs worse than the radial and axial seal geometries. Based on the curves obtained with Eq. 1, the chute, radial and axial seals are fully sealed with $U_m/(\Omega\, b)$ values of approximately 0.12, 0.05 and 0.075 respectively. The performance of the chute correlates well to the disc pumping model with $k = 1$, compared to $k = 0.4$ and $k = 0.8$ for simple radial and axial seals. However, it should be noted that the equivalent axial gap of the 1 mm tested chute seal is a factor of 2.9 higher than that found in an axial seal with a 1mm clearance. Hence, the chute seal outperforms the axial seal for the same axial seal gap, and the clearance is much less sensitive to axial movement of the rotor. The chute may also hold significant benefits over the axial and radial types, especially at high purge flow rates, for HP turbine and cycle performance and cooling.

5.2. Effect of mainstream annulus flow

The effect of the annulus flow on the sealing performance of the chute seal has been investigated for a wide range of conditions of purge flow rate, rotational speed and seal gap. In this study, the imposed annulus flow was purely axial with a Mach number of 0.34 (axial Reynolds number of $2.6\text{x}10^5$ referenced to a nominal NGV axial chord of 0.034 m), representative of a HP turbine in modern aero-engines.

The effect of the external crossflow is assessed in Figure 4(b) based on the sealing effectiveness at radial position $r/b = 0.96$ for both gap sizes without and with the annulus flow. Good agreement between the small seal clearance data without external flow (shown by filled blue triangles) and the analytical prediction from Eq.1 with $k = 1$ is evident. The same trend is largely observed in the presence of external flow (shown by filled red circles) until departure above $U_m/(\Omega b) \approx 0.06$. Beyond this point the data shows the seal is never fully sealed even at $U_m/(\Omega b) \approx 0.275$, suggesting that the complex interaction of purge and mainstream flows will always lead to some levels of ingestion at the rim. The larger scatter in the results at $\text{Re}_{ax} = 2.6\text{x}10^5$ and differences between the datasets at high sealing effectiveness indicate higher interaction between purge and annulus flows. This is suspected to be due to shear effects, and possibly small non-uniformities around the annulus when the external flow is introduced. These observations are consistent with the findings of other research groups for different seal types illustrating the complexity of the flow.

5.3. Effect of seal clearance

The results for the large seal clearance (empty markers) display a different nature. Without the external flow, the data again trend well with the plotted correlation although they sit above the analytical prediction. The 1.85 mm seal clearance was achieved by axially displacing the rotor disc rearwards. As a consequence, the overlap in the chute seal was lost. This change in configuration intrinsically modified the rim seal geometry. The sealing effectiveness data obtained with the larger gap suggest a superior sealing capability of the open seal clearance (based on the same minimum clearance) of the open seal geometry. However, because the axial displacement increases the seal clearance, it does result in more flow being required to seal the cavity. With the introduction of external flow in the larger gap set up, an improved seal performance is evident especially at high purge flow rates, however, scatter in the data at conditions with high sealing effectiveness makes it difficult to conclude the value of $U_m/(\Omega b)$ for a fully sealed cavity.

5.4. Effect of purge flow

Radial distributions of sealing effectiveness on the stator wall are shown in Figure 5(a) and (b) for $s_c = 0.0042$ and $s_c = 0.0078$ respectively, without and with annulus flow for purge flows varying from $U_m/(\Omega b) = 0.02$ to 0.09 ($C_w = 850$ to 3400) at constant rotational Reynolds number $\text{Re}_\emptyset = 1.5\text{x}10^6$. An increase in sealing effectiveness is observed as purge mass flux increases since the cavity pressure

must rise to pass more mass flow through the seal area, subsequently inhibiting ingestion. A decrease in sealing effectiveness for the larger seal gap is evident comparing data for constant $C_w = 850$ (blue markers) between the two plots.

The radial distribution of sealing effectiveness can be explained by the cavity flow structure. According to the study presented by Daily and Nece [13] turbulent flow and separate boundary layers are expected to develop inside the cavity. When ingestion occurs, the external flow that reaches the cavity mixes with the outward purge flow in the outer part of the volume. The combined flow then merges with the stator boundary layer and migrates radially downwards. Regarding Figure 5(a), a constant radial distribution of sealing effectiveness is observed in the inner part of the cavity ($r/b < 0.94$) indicating that the flow is fully mixed all along the stator boundary. On the contrary, at higher radii ($r/b > 0.94$) radial variations in the sealing effectiveness distribution indicate partial mixing of the ingested and cavity flows. It is also worth noting that the geometrical discontinuity of the stator wall joining the flat vertical and angled faces at $r/b = 0.94$ aids this affect and the trend change consistently takes place at this radial coordinate. The effect also intensifies with increasing purge flow.

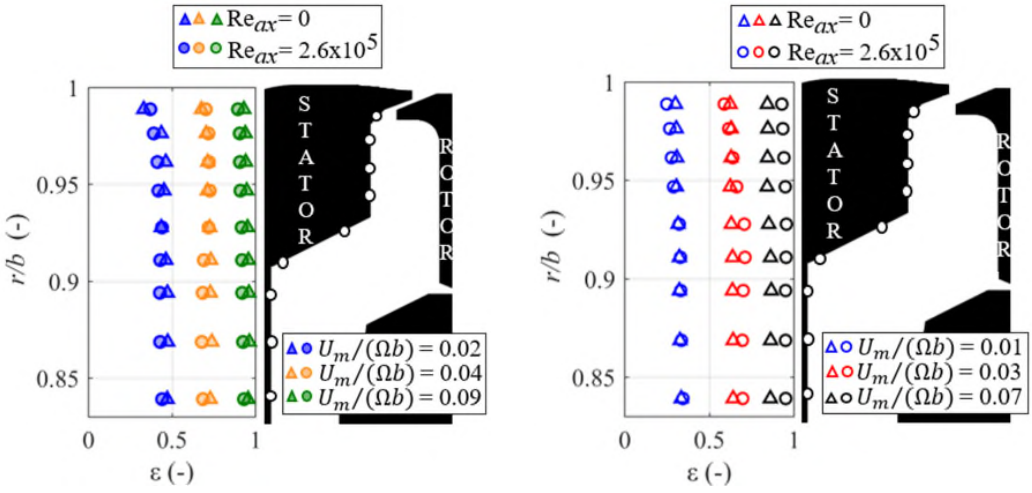

(a) (b)

Figure 5: Effect of the sealing mass flux on the sealing effectiveness radial distribution at $\mathrm{Re}_\emptyset = 1.5\mathrm{x}10^6$ without and with annulus flow for: (a) $s_c = 0.0042$, (b) $s_c = 0.0078$.

The effect of imposing the mainstream annulus flow is generally consistent for both seal gap sizes. At low purge flow rates, for example $U_m/(\Omega b) = 0.02$, the effect is small, with a consistent decrease in effectiveness near the rim seal in the mixing region between $0.94 < r/b < 0.99$. For the smaller gap size, the largest change in effectiveness, ~ 0.03, is observed at $r/b = 0.99$.

As the purge flow is increased, the effect of the mainstream flow is more significant for both seal gaps although it is more pronounced for $s_c = 0.0078$ due to the larger supply of purge flow. For $U_m/(\Omega b) > 0.04$ in Figure 5(b), the change in seal effectiveness at the rim is small, but a positive shift in seal effectiveness is observed in the fully mixed region below $r/b < 0.94$. In combination, this results in a gradient change in the mixing region between $0.94 < r/b < 0.99$. This shift in the lower cavity region was observed for both seal gaps. Interestingly, the shift also appears to increase with the rate of purge flow; at $r/b = 0.84$, the shift increases from 0.06 at $U_m/(\Omega b) = 0.04$ to 0.11 at $U_m/(\Omega b) = 0.07$.

The observed changes in seal effectiveness – small decreases near the rim at low purge flows and comparatively large positive shifts in the lower cavity at higher purge – show the addition of an external axisymmetric flow can infer a beneficial or detrimental effect in the rim seal performance depending on the seal-to-axial mass flux ratio and radial position. This improvement in sealing capability in the presence of external flow could be a consequence of the flow recirculation in the rim seal region due to the interaction between purge and annulus flows that intensifies at higher rates of sealing air supply. It is clear that the combination of the purge and annulus flows enhances the complexity of the flow structure in the rim region and inside the cavity.

CONCLUSIONS

The capability of the Oxford Rotor Facility has been enhanced to investigate the phenomena of hot gas ingestion following the findings reported by Beard *et al.* [11]. The air supply system has been upgraded, the instrumentation resolution inside the cavity increased and the working section modified with a reduced annulus casing line.

Steady pressure measurements in the current experiments revealed the presence of different core swirl velocities in the inner and outer parts of the cavity. A gas concentration measurement system to assess the sealing performance has been installed and commissioned. Sealing effectiveness data for a chute seal under purely rotationally-induced ingestion have been reported for the first time. The effect of the annulus flow on seal performance has proven to be very complex and heavily dependent on the test conditions, challenging extrapolation of some of the observed trends.

Results of sealing effectiveness have been compared to those for axial and radial seal designs available in published literature. The capability of the chute seal studied here to protect the cavity by preventing ingestion was lower than expected, showing worse sealing performance than previously reported for an axial seal. The experimental seal effectiveness data at r/b = 0.96 matched well to the analytical correlation by Chew [2] with an empirical constant of k = 1. Based on the axial gap of the chute seal, the chute geometry outperforms an axial seal of the same equivalent axial clearance and presents lower sensitivity to rotor axial displacement. The chute may also hold significant benefits over the axial and radial types, especially at high purge flow rates, for minimising secondary flows and mixing losses in the turbine and potentially providing benefits for thermal management of the HP turbine thereby aiding component life.

The results presented here build directly on those by Beard *et al.* [11], and are the first part of a wider study of rim sealing flow physics. Further experimental results, showing the effects of including NGVs in the annulus are to be presented in Bru Revert *et al.* [14]. Complementary CFD results for the chute seal considered here are given in references [15] and [16].

ACKNOWLEDGEMENTS

The research presented here has been funded by Rolls-Royce and Innovate UK through the TSB 113076 grant. The authors also wish to acknowledge the guidance provided by Peter Smout as well as the technical support of Gregory King, Sunny Chana and James Carter.

NOMENCLATURE

b	disc radius, m
c	tracer gas concentration, %
C_{ax}	axial chord, m
C_d	discharge coefficient
C_w	non-dimensional purge flow rate $= \dot{m}/\mu b$
C_p	cavity pressure coefficient $= (p - p_{1011})/0.5\rho(\Omega b)^2$
d	diameter, m
g	rim seal gap size, m
k	empirical constant
$\dot{m}$	mass flux, kg s^{-1}
M	Mach Number
p	pressure, bar
Re_{ax}	axial flow Reynolds number $= \rho U_{ax} C_{ax}/\mu$
$\mathrm{Re}_{\emptyset}$	rotational Reynolds number $= \rho\Omega b^2/\mu$
s_c	seal clearance $= g/b$
T	temperature, K
U_{ax}	axial velocity, m s^{-1}
U_m	mean flow velocity through seal in *r*-*z* plane, $= \dot{m}/\rho 2\pi b s_c$, m s^{-1}

Greeks

ε	sealing effectiveness
λ_T	turbulent flow parameter $= C_w/\mathrm{Re}_{\emptyset}{}^{0.8}$
μ	dynamic viscosity, Pa s
ρ	fluid density, kg m^{-3}
Ω	angular rotational speed, rad s^{-1}

Subscripts

0	total conditions
ann	annulus value
ax	axial component value
min	minimum value
purge	purge flow value
stator	stator wall value

Abbreviations

CFD	Computational Fluid Dynamics
HP	High Pressure
NGV	Nozzle Guide Vane
ORF	Oxford Rotor Facility

REFERENCES

[1] Bayley, F. J., and Owen, J. M., 1970, "The Fluid Dynamics of a Shrouded Disk System With a Radial Outflow of Coolant." ASME. *J. Eng. Power*. July 1970; 92(3): 335–341. https://doi.org/10.1115/1.3445358
[2] Chew, J. W., 1991, "A Theoretical Study of Ingress for Shrouded Rotating Disk Systems With Radial Outflow." ASME. *J. Turbomach*. January 1991; 113(1): 91–97. https://doi.org/10.1115/1.2927742
[3] Chew, J. W., Dadkhah, S., and Turner, A. B., 1992, "Rim Sealing of Rotor–Stator Wheelspaces in the Absence of External Flow." ASME. *J. Turbomach*. April 1992; 114(2): 433–438. https://doi.org/10.1115/1.2929162
[4] Abe, T., Kikuchi,J., and Takeuchi, H., 1979, "An Investigation of Turbine Disc Cooling (Experimental Investigation and Observation of Hot Gas Flow into a Wheel Space)." In: *Third CIMAC congress*, Vienna, paper no. GT30.
[5] Phadke, U. P., and Owen, J. M., 1983, "An Investigation of Ingress for an "Air-Cooled" Shrouded Rotating Disk System With Radial-Clearance Seals." ASME. *J. Eng. Power*. January 1983; 105(1): 178–182. https://doi.org/10.1115/1.3227382
[6] Green, T., and Turner, A.B., 1994, "Ingestion Into the Upstream Wheelspace of an Axial Turbine Stage." *J. Turbomach.*, 116(2): 327-332, doi: 10.1115/1.2928368
[7] Johnson, B.V., Mack, G.J., and Paolillo, R.E., 1994, "Turbine rim seal path flow ingestion mechanisms." AIAA paper 94.
[8] Cao, C., Chew, J.W., Millington, P.R., and Hogg, S.I., 2004, "Interaction of Rim Seal and Annulus Flows in an Axial Flow Turbine." ASME. *J. Eng. Gas Turbines Power*, 126(4): 786-793, doi: 10.1115/1.1772408
[9] Scobie, J.A., Sangan, C.M., Owen, M., and Lock, G.D., 2016, "Review of Ingress in Gas Turbines." ASME. *J. Eng. Gas Turbines Power*, 138(10): 120801, doi: 10.1115/1.4033938
[10] Chew, J.W., Gao, F., and Palermo, D.M., 2018, "Flow mechanisms in axial turbine rim sealing." *Proc. Inst. Mech. Eng. Pt. C J. Mechan. Eng. Sci.*, doi: 10.1177/ 0954406218784612
[11] Beard, P. F., Gao, F., Chana, K. S., and Chew, J., 2016, "Unsteady Flow Phenomena in Turbine Rim Seals." ASME. *J. Eng. Gas Turbines Power*. March 2017; 139(3): 032501. https://doi.org/10.1115/1.4034452
[12] Sangan, C.M., Pountney, O.J., Zhou, K., Wilson, M., Owen, J. M. and Lock, G. D., 2013, "Experimental Measurements of Ingestion Through Turbine Rim Seals. Part II: Rotationally Induced Ingress." ASME. *J. Turbomach*., 135(2): 021013, doi: 10.1115/1.4006586
[13] Daily, J.W., and Nece, R.E., 1960, "Dimension Effects on Induced Flow and Frictional Resistance of Enclosed Rotating Discs." ASME. *J. Basic Eng.* 82(1): 217-230: doi: 10.1115/1.3662532
[14] Bru Revert, A., Beard, P.F., Chew, J.W., Bottenheim, S., 2020, "Performance of a Turbine Rim Seal Subject to Rotationally-Driven and Pressure-Driven Ingestion." Submitted to ASME TurboExpo 2020 Paper GT2020-14773.
[15] Palermo, D. M., Gao, F., Chew, J.W. and Beard, P. F., 2019, "Effect of Annulus Flow Conditions on Turbine Rim Seal Ingestion.", ASME Turbo Expo 2019 Paper GT2019-90489, doi: 10.1115/GT2019-90489
[16] Palermo, D. M., Gao, F., Amirante, D., Chew, J.W, Bru Revert, A. and Beard, P.F., 2020, "Wall Modelled Large Eddy Simulations of Axial Turbine Rim Sealing With Unstructured Linear Reconstruction Techniques." Submitted to ASME TurboExpo 2020 Paper GT2020-14973.